Available online at www.sciencedirect.com
ScienceDirect
Journal of Power Sources 169 (2007) 9–16
JOURNAL OF POWER SOURCES
www.elsevier.com/locate/jpowsour

Catalytic properties of monometallic copper and bimetallic copper-nickel systems combined with ceria and Ce-X (X = Gd, Tb) mixed oxides applicable as SOFC anodes for direct oxidation of methane☆

A. Hornés[a], D. Gamarra[a], G. Munuera[b], J.C. Conesa[a], A. Martínez-Arias[a,*]

[a] *Instituto de Catálisis y Petroleoquímica, CSIC, C/Marie Curie 2, Campus de Cantoblanco, 28049 Madrid, Spain*
[b] *Departamento de Química Inorgánica e Instituto de Ciencia de Materiales (Centro Mixto Universidad de Sevilla-CSIC), 41092 Sevilla, Spain*

Available online 6 February 2007

Abstract

The present contribution analyses the possibilities of both Cu and bimetallic Cu-Ni formulations combined with CeO_2-based oxides for their use as anodes of solid-oxide fuel cells (SOFC) for direct oxidation of methane. The main objective is related to examining how the metals combination and the presence of dopants like Gd and Tb into the ceria structure could affect the catalytic activity of this type of materials towards reaction with methane. For this purpose, cermets of Cu alone as well as bimetallic Cu-Ni (with 20 and 40 wt.%) have been synthesised in combination with various supports composed by oxides of Ce, Ce-Tb and Ce-Gd. The behaviour of such systems towards interaction with dry methane up to 900 °C was analysed by means of CH_4-TPR tests. Appreciable differences in the catalytic activity are revealed as a function of the presence of nickel as well as Gd or Tb dopants in the systems. The characteristics of carbonaceous deposits formed upon such interaction was analysed by means of TPO and XPS.

Keywords: SOFC; Anode; Direct oxidation of methane; Intermediate temperature; Copper; Nickel; CeO_2; CGO; Ce-Tb mixed oxide

1. Introduction

Solid oxide fuel cells (SOFC) are galvanic devices most interesting from environmental and energetic points of view due to their high efficiency for conversion from chemical to electrical energy and their high versatility towards employment of various types of fuels [1]. Classical systems of this type involve the employment of thin YSZ electrolytes with an anode based on Ni-YSZ cermets and can attain an energetic efficiency close to 70% operating at relatively high temperature (800–1000 °C) with hydrocarbon reforming mixtures as fuel [1–3]. This efficiency can be theoretically increased by employing direct hydrocarbon oxidation conditions instead of fuel mixtures resulting from reforming [4]. However, the classical anode of nickel could easily be deactivated under those conditions as a consequence of the formation of carbonaceous deposits due to the relatively good activity of nickel for hydrocarbon cracking [5–8]. Different alternatives were developed in this respect to overcome such deactivating effect. Murray et al. successfully operated a cell on dry methane by employing a nickel-containing ceria-based anode at relatively low reaction temperature (650 °C) [6]. In turn, such ceria-containing anode could in principle be compatible with electrolytes able to operate at intermediate temperatures (500–700 °C) like gadolinium-doped ceria (CGO) [1]. However, the nickel-based anode can be limited when less refractory (and therefore more easy to be cracked) hydrocarbons are employed as fuel [5,7,8].

A more versatile alternative was developed by Gorte, Vohs and col. and consisted in employing anodes including mixtures between copper and cerium oxide [5,7,9–16]. Such configuration has demonstrated to be able to employ a large diversity of hydrocarbon fuels (methane or longer chain ones and even aromatics) under direct oxidation conditions and displaying a reasonable stability [4,7,11]. However, the copper anode can present several limitations related to its relatively low melting temperature, which can make difficult the fabrication of Cu cermets and can also affect the anode stability when operating at high temperature [16,17] (although it could perform

☆ This paper presented at the 2nd National Congress on Fuel Cells, CONAPPICE 2006.

* Corresponding author. Tel.: +34 91 585 4940; fax: +34 91 585 4760.
E-mail address: amartinez@icp.csic.es (A. Martínez-Arias).

0378-7753/$ – see front matter © 2007 Elsevier B.V. All rights reserved.
doi:10.1016/j.jpowsour.2007.01.074

well at intermediate temperatures), and poor performance for hydrocarbon activation [4,16].

In this context, the present work intends to study the catalytic properties of different anode configurations for direct methane oxidation and using the basic copper-ceria configuration as the starting reference material. This is compared with bimetallic Cu-Ni configurations, considering the higher thermal stabilities and chemical reactivity of nickel with respect to copper. Modifications of the transport (electrical) or redox properties of ceria by employment of structurally related mixed oxides upon doping with Gd and Tb are also expected [18]; in this respect, a previous work of our group demonstrated that doping of ceria with Tb induces changes in the type of conductivity while it made the system somewhat more stable towards thermal sintering [19]. Catalysts synthesized by two different methods (in order to achieve different components configurations which could be most relevant to the anode performance [17]) were characterized by XRD, XPS and S_{BET} and analysed with respect to their catalytic activity by means of TPR tests under dry methane. In turn, since generation of carbon deposits during direct hydrocarbon interaction must strongly affect the SOFC performance (in general they will poison the anode although in some bimetallic Cu-M configurations they have also eventually displayed positive effects attributed to increased electrical conduction as a consequence of an enhanced connectivity at microscopic level between metal particles in the anode [4]) and their characteristics are expected to be affected by chemical changes in the anode components, these have been explored by TPO and XPS.

2. Experimental

2.1. Materials

Several potential materials to be used as SOFC anodes combining Cu and Cu-Ni with CeO_2, $Ce_{0.9}Gd_{0.1}O_{2-x}$ and $Ce_{0.8}Tb_{0.2}O_{2-y}$ were prepared by two different methods: coprecipitation within reverse microemulsions and incipient wetness impregnation. For the coprecipitation within microemulsions, two reverse microemulsions, of similar characteristics concerning the volumes employed of organic (n-heptane) and aqueous phases as well as surfactant (Triton X-100) and co-surfactant (1-hexanol), were prepared; details on this can be found elsewhere [20]. The first one contained in its aqueous phase the dissolved (nitrate) salts of Ce, Gd, Tb, Cu or Ni while the second one contained in its aqueous phase a dissolved base (tetramethyl ammonium hydroxide or TMAH) which is employed as precipitating agent. Mixing both microemulsions produces the precipitation of the cations and after separation of the solid by centrifugation and decanting, the resulting solid is rinsed with methanol and dried for 24 h at 100 °C. The resulting material is then calcined under air initially at 500 °C during 2 h and finally at 950 °C during 2 h, employing relatively slow heating ramps of $2^\circ\ min^{-1}$. The latter calcination temperature is essentially determined by the minimum temperature required finally to conform monocells having this type of anode over CGO electrolyte membranes [21]. The second preparation method consisted in the (incipient wetness) impregnation of the aqueous salts of the metals (Cu and Ni) over CeO_2, $Ce_{0.9}Gd_{0.1}O_{2-x}$ and $Ce_{0.8}Tb_{0.2}O_{2-y}$ previously prepared by the microemulsion method and calcined at 500 °C. Following the impregnation and drying of the systems at 100 °C, the catalysts with the metals dispersed on their surface were calcined at 500 °C and finally at 950 °C under the same conditions employed in the first method. In any of the cases, samples with total metal loadings of 20 and 40 wt.% (with 1/1 atomic ratios for bimetallic Cu-Ni systems) have been analysed. Similar microemulsion-precipitation methods were employed to prepare reference CuO or CeO_2 with a final calcination being performed at 950 °C. Chemical analyses of the samples by ICP-AES demonstrated quantitative precipitation in any of the samples, the actual contents of any component being the same (within experimental error) as the nominal values employed. The samples will be denoted hereafter as *x*M-C, *x*M-CG and *x*M-CT (with $x = 20$ or 40, depending on the metal wt.% and M = Cu or Cu-Ni) depending on whether the support material is CeO_2, $Ce_{0.9}Gd_{0.1}O_{2-x}$ or $Ce_{0.8}Tb_{0.2}O_{2-y}$, respectively. The samples prepared by impregnation will be referred to with a /I suffix.

2.2. Techniques

Specific surface area (S_{BET}) determination was made from curves of adsorption/desorption of N_2 at 77 K over the samples outgassed at 140 °C using a Micromeritics ASAP 2100 equipment.

Powder XRD patterns of the samples were recorded on a Seifert XRD 3000P diffractometer using nickel-filtered Cu Kα radiation operating at 40 kV and 40 mA, using a 0.02° step size and 2 s counting time per point.

X-ray photoelectron spectra (XPS) were recorded with a Leybold-Heraeus spectrometer equipped with an EA-200 hemispherical electron multichannel analyzer (from Specs) and a 120 W, 30 mA Mg Kα X-ray source. The samples (0.2 mg) were slightly pressed into a small (4 mm × 4 mm) pellet and then mounted on the sample rod and introduced into the pretreatment chamber where they could be subjected in situ to thermal or redox treatments under ca. 1 Torr of reactive gases (i.e. 20% CH_4/He mixture). Following each treatment, the sample was moved into the ion-pumped analysis chamber where it was further outgassed until a pressure less than 2×10^{-9} Torr was attained (2–3 h.). This low pressure was maintained during all the data acquisition by ion pumping of the chamber. After each treatment, XP spectra in the relevant energy windows were collected for 20–90 min, depending on the peak intensities, at a pass energy of 44 eV (1 eV = 1.602×10^{-19} J) which is typical of high resolution conditions. The intensities were estimated by calculating the integral of each peak after subtraction of an S-shaped Shirley-type background with the help of UNIFIT for Windows (Version 3.2) software [22]; atomic ratios were then derived using the appropriate experimental sensitivity factors. All binding energies (BE) were referenced to the Ce(3d) u‴ line at 917.0 eV which, as we have previously shown [23], gives a value of 284.6 ± 0.1 eV for the adventitious graphitic C(1s) line.

Temperature programmed reduction (TPR) tests under diluted dry methane (5% CH_4/He) were done in a quartz flow

microreactor filled with about 500 mg of sample and employing 150 mL min^{-1} total flow. Heating ramps of 10 °C min^{-1} from 30 to 900 °C, maintaining finally this temperature for 2 h under the reactant mixture (enough in all cases for achieving stabilization of the reaction products), were used. Subsequently, the sample was cooled under the same flow and after extensive purging under He at 30 °C, they were subjected to a temperature programmed oxidation (TPO) test under 5% O_2/He (using the same flow rate as for the TPR tests) up to 900 °C (10 °C min^{-1} ramp) and keeping this temperature until products stabilization. Gases evolving from the reactor were analysed with a Pfeiffer Omnistar quadrupolar mass spectrometer.

3. Results and discussion

Specific surface area values obtained for all the samples reveal a significant sintering upon calcining the samples at 950 °C (S_{BET} values between <0.5 and 1.6 m^2 g^{-1}) with respect to the samples calcined at 500 °C (S_{BET} values between 50.0 and 100.0 m^2 g^{-1}). Nevertheless, CG- and CT-supported samples apparently maintain after calcination at 950 °C relatively higher surface areas (with values higher than 1 m^2 g^{-1}) than the C supported ones (having in all cases S_{BET} < 0.5 m^2 g^{-1}), thus revealing that doping with Gd or Tb helps to stabilize somewhat the systems towards thermal sintering, in agreement with previous findings [19]. The presence of the metals apparently can also have a role on this since higher surface areas are detected after sintering for the samples with 40 wt.% metal content than for those with 20 wt.%.

As illustrated in Fig. 1, the X-ray diffractograms of the initial samples calcined at 950 °C display mainly peaks due to the fluorite phase of either CeO_2 or Gd- or Tb-doped ceria [24,25]. In addition, the copper containing samples display the presence of tenorite CuO. In this respect, it is interesting that CuO peaks are apparently more intense for samples prepared by impregnation than for those prepared by microemulsion–coprecipitation, thus indicating that the latter preparation method favours introduction

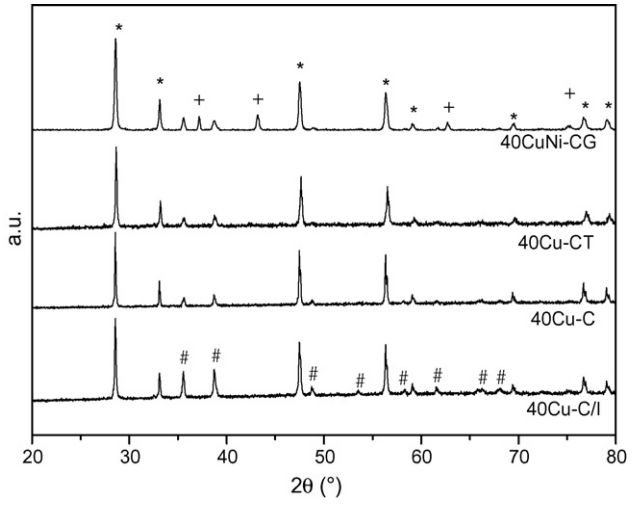

Fig. 1. X-ray diffractograms of the indicated systems calcined at 950 °C. Peaks attributions is as follows—(*) fluorite CeO_2, $Ce_{0.8}Tb_{0.2}O_{2-x}$ or $Ce_{0.9}Gd_{0.1}O_{1.95}$ phases; (#) tenorite CuO; (+) NiO.

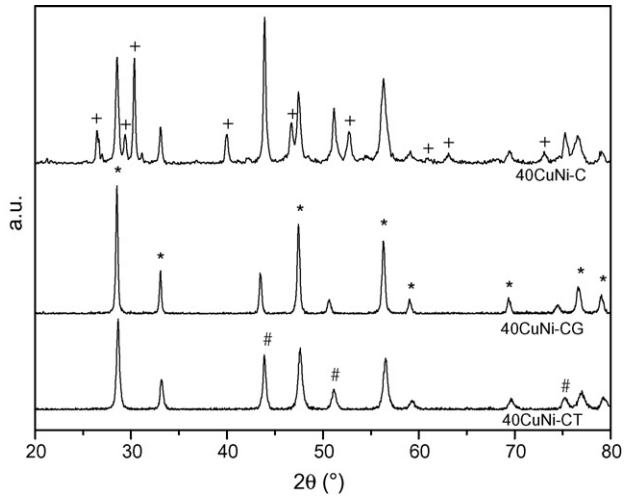

Fig. 2. X-ray diffractograms of the indicated catalysts after TPR under diluted CH_4 up to 900 °C. Assignments—(*) fluorite cerium oxide (or Ce-Gd or Ce-Tb mixed oxide) phases; (+) Ce_2O_3; (#) CuNi alloy.

of a part of the copper into the fluorite structure, in agreement with previous investigations [26]. In the case of the nickel containing samples, the presence of a NiO phase is apparent and no mixed oxide with copper appears to be formed.

However, important changes were detected in the X-ray diffractograms of the samples subjected to TPR under diluted methane up to 900 °C. This has been examined in all samples of the bimetallic CuNi series and is illustrated in Fig. 2 for the samples with 40 wt.% metal loadings. Noteworthy, as it occurs also for the 20 wt.% loading samples, a reduced hexagonal Ce_2O_3 phase becomes stabilized in air in the absence of doping with either Gd and Tb, indicating that the latter are able to stabilize fluorite phases of the support, most likely related to highly oxidised states. Concerning the metal component, all three cases show the formation of a CuNi alloy (on the basis of the shift observed in the peaks with respect to positions expected for the pure metals) which appears more enriched in copper for the CG-supported catalyst. This in turn suggests that this latter may present a surface enrichment in Ni for this alloy.

The evolution of CO_2 during CH_4-TPR tests for different copper catalysts and reference samples are shown in Fig. 3. Fairly similar results were observed when comparing the positions of reduction peaks observed for samples with 20 and 40 wt.% loading of metal (the former generally showing, as expected, lower intensity). We will therefore centre the discussion on the latter, which appears most interesting from a practical point of view [4]. It is observed that methane does not begin to react evolving CO_2 in any of the cases until ca. 600 °C are attained, which contrasts with results observed for samples of this kind in a less sintered state (calcined only at 650 °C), for which methane oxidation was observed at lower temperature [27]. In our samples, comparison with CuO and CeO_2 reference samples suggests that it is essentially the copper oxide component of the systems which can be involved in the methane oxidation process. No particular decrease of the reaction temperature is observed in the Cu-C sample. These results contrast with those observed for less sintered samples of copper oxide dispersed on ceria (weakly doped

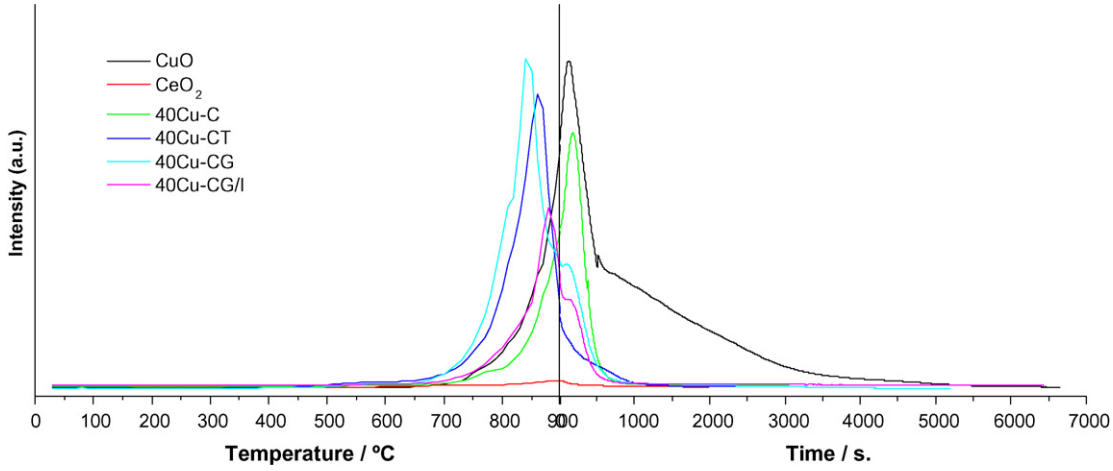

Fig. 3. Evolution of the $m/e = 44$ MS signal during CH_4-TPR tests over the indicated catalysts.

with lanthanum), in which promoting effects of dispersed copper oxide entities on ceria reduction upon interaction with methane were claimed to occur and attributed to closer copper-ceria interactions in samples with higher surface area [27]. In our case, interestingly promoting effects for the reduction are observed for highly sintered samples when either Ce-Gd or Ce-Tb mixed oxides are employed as supports, suggesting a strong relevance of enhanced transport properties in the methane oxidation process [24]. On the other hand, comparison between the most active Cu-CG catalyst prepared by microemulsion–precipitation and impregnation methods indicates the higher activity of the former, thus indicating that introduction of copper into the fluorite structure can be most relevant to increase the oxidative activity of the samples.

As shown in Fig. 4, a general decrease in the methane oxidation temperature is observed for the bimetallic CuNi systems with respect to the monometallic Cu ones, in consistency with the higher expected reactivity of nickel towards methane [5–8]. Appreciable support promotion effects are also observed for these bimetallic systems. In particular, the promoting effect on the methane oxidation follows the order CuNi-CG > CuNi-CT > CuNi-C. In addition to support effects on the oxidation process (as also observed for the monometallic copper ones, Fig. 3) the nature of the CuNi alloy formed in each case can also play a significant role on the catalytic properties of these systems as will be analysed below.

A complete analysis of all the gases evolving during these CH_4-TPR experiments gives important hints on the processes taking place in the course of the test. As shown in Fig. 5, in which the test performed over the original oxidised CuNi-CG sample is displayed, the process of total methane oxidation ($CH_4 + 4O_{solid} \rightarrow CO_2 + 2H_2O$) prevails at lower temperature (between ca. 550 and 800 °C) at which reduction of Ni (and probably also of Cu) to the metal state has not yet been completed and thus carbon deposition is unlikely to be significant. This agrees with previous proposals suggesting that these systems could favour total oxidation under real SOFC operating conditions when oxygen transport is fast enough to provide oxygen to the methane molecules [4]. For temperatures approaching 900 °C at which the catalyst has certainly become reduced, partial oxidation processes ($CH_4 + O_{solid} \rightarrow CO + 2H_2$, $CH_4 + 2O_{solid} \rightarrow CO + 2H_2O$) are clearly revealed while probably methane cracking and generation of carbon deposits ($CH_4 \rightarrow C + 2H_2$) likely occur also at those temperatures. This

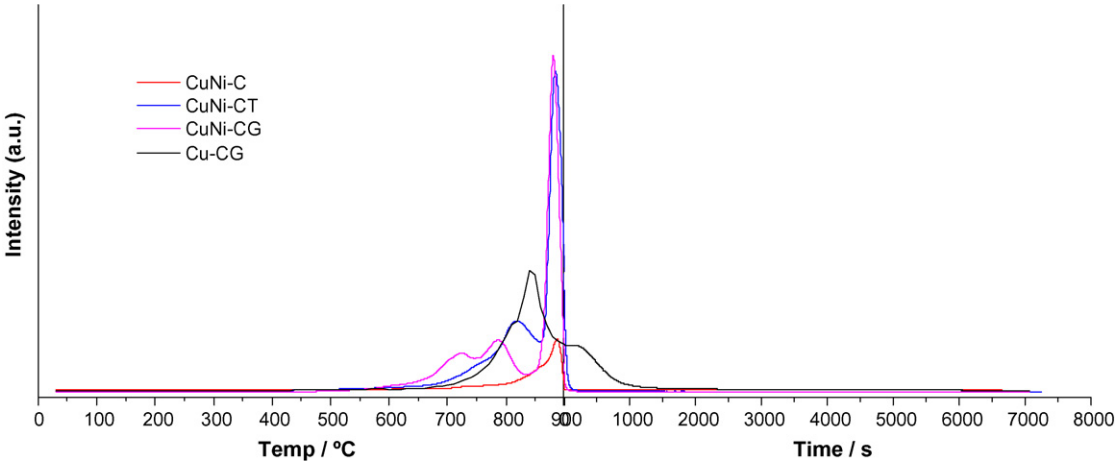

Fig. 4. Evolution of the $m/e = 44$ MS signal during CH_4-TPR tests over the indicated catalysts.

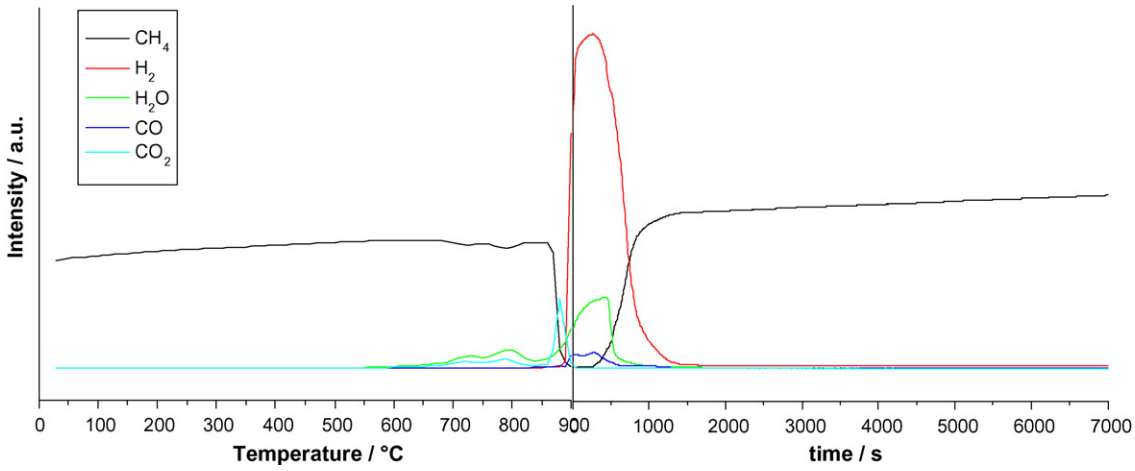

Fig. 5. Evolution of the $m/e = 2$, 16, 18, 28 (corrected to eliminate the contribution to this signal from CO_2) and 44 MS signals (corresponding to the indicated gases) during the CH_4-TPR tests over the CuNi-CG oxidised sample.

latter partial reduction and methane cracking processes are favoured over the prereduced catalyst, as clearly revealed in Fig. 6.

TPO tests subsequent to the CH_4-TPR tests clearly reveal the generation of carbon deposits during these tests. As displayed in Fig. 7, the amount of carbon deposited is apparently higher in the presence of nickel, as expected from the mentioned higher reactivity of this latter towards methane [4–8]. It is also interesting in this respect the comparison between CuNi-CG and CuNi-C in which an appreciably higher amount of CO_2 is shown to evolve for the former (Fig. 7). This correlates well with the mentioned differences in the CuNi alloy formed in each case which appears more enriched in Ni for the former which could also favour a higher reactivity towards methane in it. Nevertheless, it can be also appreciated that upon the high temperature interaction with methane, the carbon deposits formed in copper only samples are very stable (even if in small amount), while for the bimetallic samples (and among them for the CuNi-CG sample, most active in this respect) they appear to be considerably less stable (more easy to oxidise). The fact that in the latter sample the oxidation of carbon in this TPO run is seen to be completed efficiently already at $T < 650\,^{\circ}C$ suggests that this type of composition (bimetallic CuNi particles on Gd-doped ceria), under fuel cell operation conditions (with steady state supply of oxygen from the electrolyte), could be effective for keeping relatively low levels of carbon deposited on the anode. In contrast, the samples containing only copper apparently form considerably lower amounts of carbon deposits and these could correspond to very stable forms of carbon upon the high temperature interaction with methane.

In order to get more hints on the nature of carbon deposits formed in the latter type of samples (Cu-C and Cu-CT), they have been explored after the CH_4-TPR treatment up to 900 °C for the 40 Cu-C and 40 Cu-CT samples by XPS. As shown in Fig. 8 substantial differences are appreciated in the XPS spectra in the C(1s) region (ca. 300-270 eV) for either of the two original samples or when they had been treated under CH_4 up to 900 °C. Besides the lines at ca. 289.0 and 285.7 eV due respectively to the Ce(4s) and Tb(4p) photoemissions, the spectra of both samples after the CH_4-TPR run, display overlapped on those signals an intense and sharp peak at ca. 286.0 eV and a somewhat smaller one at ca. 289.0 eV. Moreover, in the case of

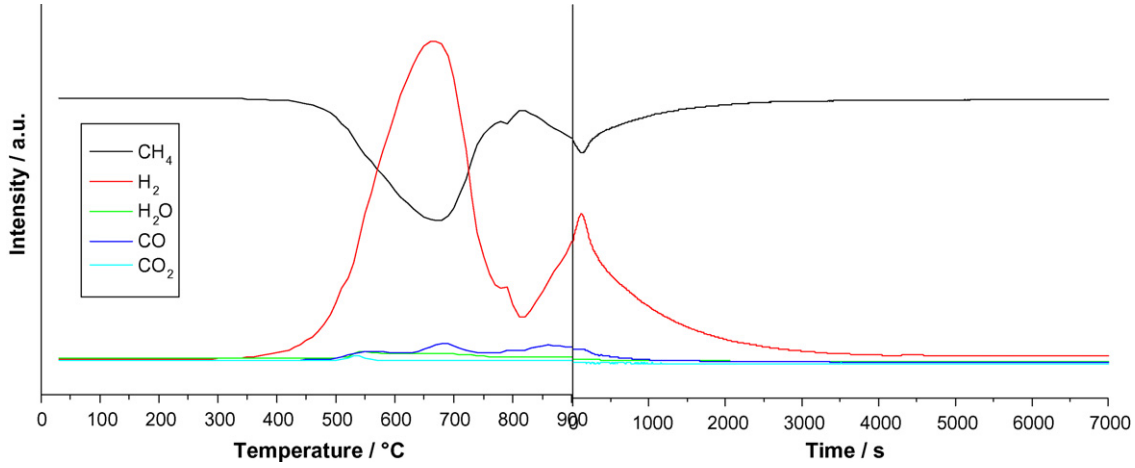

Fig. 6. The same as Fig. 5 over the CuNi-CG sample prereduced under diluted H_2 at 500 °C.

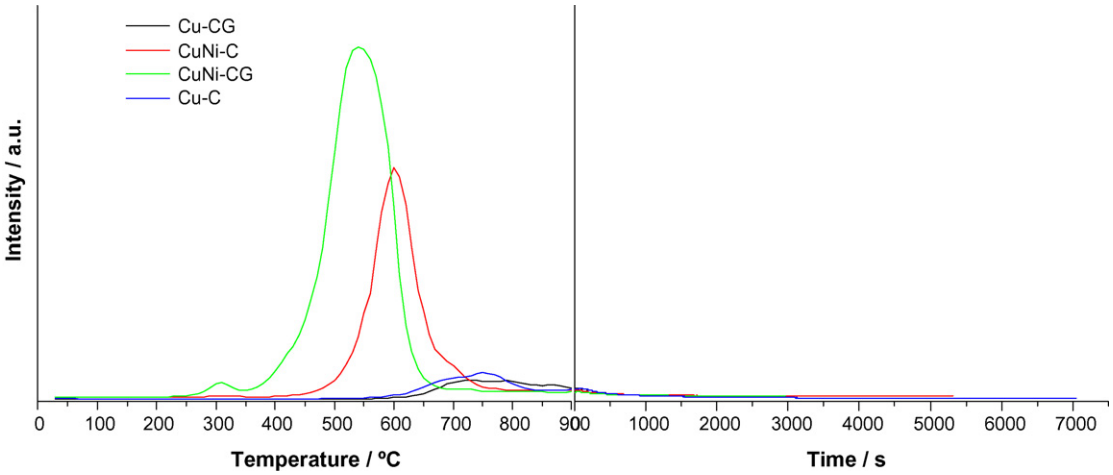

Fig. 7. Evolution of the $m/e = 44$ MS signal during TPO tests subsequent to CH_4-TPR tests over the indicated catalysts.

sample 40 Cu-C, a completely new sharp peak, at ca. 280.9 eV appears. Taking into account that the reference graphitic carbon would appear at ca. 284.6 eV (and might be also overlapped to the 286.0 eV peak in the spectrum of the samples treated under CH_4), the signal appearing at 289.0 eV must correspond, as reported in the NIST XPS database [28], to oxidised carbonaceous deposits while the one at 286.0 eV may well belong to oxygen bonded –[CH_2]- polymeric species. In turn, the relatively strong B.E. shift of the sharp signal observed at ca. 280.9 eV in the sample 40 Cu-C, suggests that it must be associated to some carbide-like phase of the type C_yCe or C_yCe_xCu, by analogy to well known phases such as CW, CTi or CHf [28].

On the other hand, the study of the evolution of the Cu(2p) and Cu($L_3M_{45}M_{45}$,^{1}G) lines, using Wagner's chemical state diagrams [29], shows that in the two original samples copper was 100% as Cu^{2+} while a treatment in situ (at the XPS chamber) with a 20% CH_4/He mixture at 500 °C during ca. 3 h produces only less than 10% reduction to Cu^+ and Ce^{3+} without any change in the Cu(Ce + Cu) or Cu/(Cu + Ce + Tb) atomic ratios that remain close to the 0.45 ± 0.02 original values in the two samples.

For the sample 40 Cu-CT, after the CH_4-TPR run, copper and ceria remain with the same atomic ratio and fully oxidized (remember that the sample had been exposed to the air during its transfer to the XPS chamber), the Tb(3d) signal indicates a

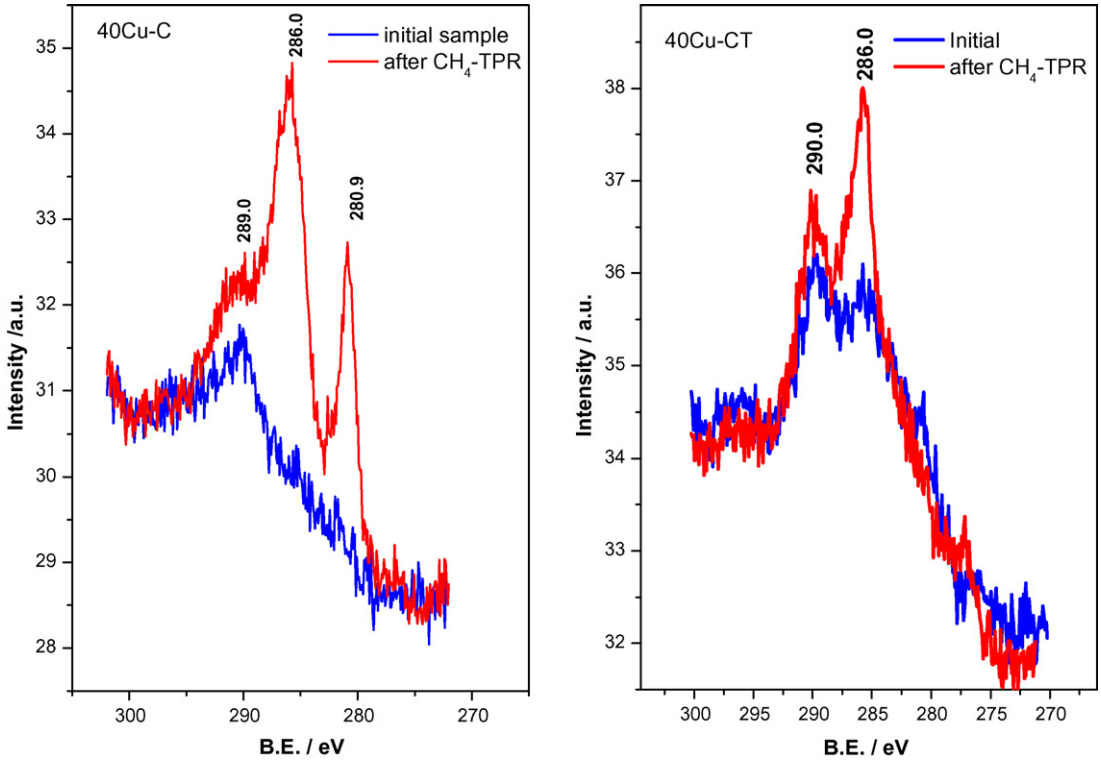

Fig. 8. XPS spectra in the C(1s) zone of the initial Cu-C sample (calcined at 950 °C) and after CH_4-TPR up to 900 °C (left). The same for the Cu-CT sample (right).

Tb^{3+}/Tb^{4+} ratio much higher than in the original sample thus suggesting an easy electron transfer from Ce^{3+} to Tb^{4+} (in other words, Tb^{4+} is reduced preferentially rather than Ce^{4+}) as we have recently reported elsewere [30]. However, in the case of the sample 40 Cu-C the Cu/(Cu + Ce) ratio increases from 0.44 up to 0.58 after the CH_4-TPR process, indicating surface segregation of copper, while the Cu(2p) photoemission shows a complex structure with a main $3d_{5/2}$ B.E. peak at 931.5 eV, shifted by −1.3 eV from metallic copper, and two shoulders at higher binding energies due to Cu^+ and Cu^{2+} species. The peak at 931.5 eV must be ascribed to some kind of alloyed copper (i.e CuPd alloy shows a shift of −0.8 eV [28]). Meanwhile, the Ce(3d) photoemission was also complex indicating the presence of low oxidized species (i.e. Ce^{3+} and/or Ce^0), which agrees with XRD data reported above. Noteworthy, strongly reduced cerium oxide can be reoxidized immediately to some extent when exposed to the air. All these facts seem to confirm the formation of the above-mentioned CCe_xCu_y alloyed carbidic phase in 40 Cu-C while the CT-based sample would be protected against such alloy formation. All these new C(1s), Cu(2p) and Ce(3d) signals could be eliminated in both samples by a short (∼30 s.) non-reductive sputtering with O_2^+ ions at 3.5 kV., recovering the spectra of the original samples, what indicates a weak bulk development of C-containing alloyed phase and of the diverse types of the carbon deposits generated upon the interaction with CH_4 up to 900 °C. In fact, the amount of C-species formed by CH_4-TPR, estimated from the relative areas of the corresponding peaks obtained by subtracting both spectra of each sample, was 5–6 times higher in the 40 Cu-C sample than in the 40 Cu-CT one. Still, it only represents a few percent of the atoms detected by XPS even in the 40 Cu-C sample treated with CH_4 at 900 °C.

4. Conclusions

Different materials involving combinations of monometallic copper and bimetallic copper-nickel combined with either ceria or Ce-Gd and Ce-Tb mixed oxides have been examined with respect to their catalytic properties towards oxidation of methane in the context of their potential application as anodes of SOFC for direct oxidation of hydrocarbons. CH_4-TPR results reveal important differences as a function of the presence of Ni as well as Gd and Tb in the systems. While, as expected, the presence of Ni appreciably enhance the methane reactivity, the doping of ceria by Gd or Tb is shown to be also generally beneficial for such reactivity as a consequence of the modifications induced in the redox or transport properties of the materials. Differences in the methane reactivity as a function of the redox state of the catalyst are also revealed. As expected, the full oxidation process is favoured when the systems are oxidised while partial oxidation and or methane cracking processes leading to carbon deposition prevail upon interaction with the reduced catalysts. The nature of such carbon deposits have been analysed by TPO and XPS and confirm that their amount increases in the presence of nickel and apparently depend on the surface characteristics of the Cu–Ni alloy formed in each case, which apparently also depend on the presence of Gd or Tb in the system. The carbon deposits are formed in considerably lower amount in the copper only systems although they form more stable deposits whose nature apparently depends also on the presence of dopants in the ceria fluorite structure. The beneficial effects on the methane activity observed in the presence of Tb or Gd dopants in ceria can be related to the stabilization of the fluorite phase in them, even after strong reduction under methane, which could also prevent the generation of carbidic alloys and facilitate also the oxidation at relatively low temperature of the carbonaceous deposits formed upon interaction with methane.

Acknowledgements

A.H. and D.G. thank the CSIC and Ministerio de Educación y Ciencia (MEC) for an I3P postgraduate and FPI Ph.D. grants, respectively. Thanks are due to the CICyT or MEC (projects MAT2003-03925 and CTQ2006-15600/BQU) and Comunidad de Madrid (project ENERCAM S-0505/ENE/000304) for financial support.

References

[1] B.C.H. Steele, A. Heinzel, Nature 414 (2001) 345.
[2] B.C.H. Steele, J. Mater. Sci. 36 (2001) 1053.
[3] J.M. Ralph, A.C. Schoeler, M. Krumpelt, J. Mater. Sci. 36 (2001) 1161.
[4] S. McIntosh, R.J. Gorte, Chem. Rev. 104 (2004) 4845.
[5] G.M. Crosbie, E.P. Murray, D.R. Bauer, H. Kim, S. Park, J.M. Vohs, R.J. Gorte. SAE Paper 2001-01-2545, 2001.
[6] E.P. Murray, T. Tsai, S.A. Barnett, Nature 400 (1999) 649.
[7] S. Park, R.J. Gorte, J.M. Vohs, Appl. Catal. A 200 (2000) 55.
[8] A.-L. Sauvet, J. Fouletier, J. Power Sources 101 (2001) 259.
[9] S. Park, R. Craciun, J.M. Vohs, R.J. Gorte, J. Electrochem. Soc. 146 (1999) 3603.
[10] R. Craciun, S. Park, R.J. Gorte, J.M. Vohs, C. Wang, W.L. Worrell, J. Electrochem. Soc. 146 (1999) 4019.
[11] S. Park, J.M. Vohs, R.J. Gorte, Nature 404 (2000) 265.
[12] R.J. Gorte, S. Park, J.M. Vohs, C. Wang, Adv. Mater. 12 (2000) 1465.
[13] H. Kim, S. Park, J.M. Vohs, R.J. Gorte, J. Electrochem. Soc. 148 (2001) A693.
[14] R.J. Gorte, J.M. Vohs, R. Craciun, Patents WO 00/52780; US 2001/0029231 A1; US 2001/0053471 A1.
[15] R.J. Gorte, H. Kim, J.M. Vohs, J. Power Sources 106 (2002) 10.
[16] R.J. Gorte, J.M. Vohs, J. Catal. 216 (2003) 477.
[17] S. Jung, C. Lu, H. He, K. Ahn, R.J. Gorte, J.M. Vohs, J. Power Sources 154 (2006) 42.
[18] M. Fernández-García, A. Martínez-Arias, J.C. Hanson, J.A. Rodríguez, Chem. Rev. 104 (2004) 4063.
[19] A. Martínez-Arias, A.B. Hungría, M. Fernández-García, A. Iglesias-Juez, J.C. Conesa, G.C. Mather, G. Munuera, J. Power Sources 151 (2005) 43.
[20] A. Martínez-Arias, M. Fernández-García, V. Ballesteros, L.N. Salamanca, J.C. Conesa, C. Otero, J. Soria. Langmuir 15 (1999) 4796.
[21] G.C. Mather (private communication).
[22] R. Hesse, T. Chassé, R. Szargan, Fresenius J. Anal. Chem. 365 (1999) 48.
[23] A. Martínez-Arias, M. Fernández-García, A.B. Hungría, J.C. Conesa, G. Munuera, J. Phys. Chem. B 107 (2003) 2667.
[24] A. Trovarelli, in: A. Trovarelli (Ed.), Catalysis by Ceria and Related Materials, Imperial College Press, 2002, p. 15, ch 2.
[25] A.B. Hungría, A. Martínez-Arias, M. Fernández-García, A. Iglesias-Juez, A. Guerrero-Ruiz, J.J. Calvino, J.C. Conesa, J. Soria. Chem. Mater. 15 (2003) 4309.

[26] X.Q. Wang, J.A. Rodriguez, J.C. Hanson, D. Gamarra, A. Martínez-Arias, M. Fernández-García, J. Phys. Chem. B 109 (2005) 19595.
[27] Lj. Kundakovic, M. Flytzani-Stephanopoulos, Appl. Catal. A 171 (1998) 13.
[28] NIST, XPS Database, Nacional Institute of Standards and Technology-US Department of Commerce, 2006, http://srdata.nist.gov/XPS.
[29] C.D. Wagner, L.H. Gale, R.H. Raymond, Anal. Chem. 51 (1979) 466.
[30] G. Munuera, A. Martinez-Arias, A.B. Hungria, J.C. Conesa, Third CONCORDE Conference on Catalytic Nano-Oxides Research and Development in Europe: Present and Future P22, Seville, Spain, May 2006.